

1 Title:

2 Estimation of γ/γ' diffusion mobility and three-dimensional phase-field simulation of rafting
3 in a commercial nickel-based superalloy
4
5
6
7

8
9 Author names:

10 Yuhki TSUKADA^{a,*}, Toshiyuki KOYAMA^a, Yoshinori MURATA^b, Nobuhiro MIURA^c, and
11
12 Yoshihiro KONDO^c
13
14
15
16
17

18 Affiliations:

19
20
21 ^a Department of Materials Science and Engineering, Graduate School of Engineering,
22 Nagoya Institute of Technology, Gokiso-cho, Showa-ku, Nagoya 466-8555, Japan
23
24

25 ^b Department of Materials, Physics and Energy Engineering, Graduate School of
26 Engineering, Nagoya University, Furo-cho, Chikusa-ku, Nagoya 464-8603, Japan
27
28

29 ^c Department of Mechanical Systems Engineering, School of Systems Engineering,
30 National Defense Academy, 1-10-20 Hashirimizu, Yokosuka 239-8686, Japan
31
32
33
34
35
36

37 *Corresponding author:

38
39 Tel.: +81-52-735-5059
40

41 Fax: +81-52-735-5124
42

43 E-mail address: tsukada.yuhki@nitech.ac.jp
44
45
46
47
48
49
50
51
52
53
54
55
56
57
58
59
60
61
62
63
64
65

Abstract

The diffusion mobility associated with γ/γ' interface migration (γ/γ' diffusion mobility) in a nickel-based superalloy is estimated on the basis of the database of multicomponent atomic diffusion mobility. The estimation is based on the assumption that the phase equilibrium is reached during high-temperature creep, and that the γ/γ' interface migration is controlled by atomic diffusion of Re, which exhibits the smallest atomic diffusion mobility in the alloy system under consideration. Utilization of the estimated γ/γ' diffusion mobility enabled a three-dimensional phase-field simulation of microstructure-dependent heterogeneous creep in the γ matrix phase, directional coarsening of the γ' precipitate (rafting), and macroscopic creep responses. The estimation of γ/γ' diffusion mobility is assumed to be effective for quantitatively analyzing the rafting kinetics during high-temperature creep by the phase-field simulation.

Keywords: phase-field model; nickel-based superalloy; creep; plasticity; directional coarsening; diffusion

1. Introduction

Nickel-based single-crystal superalloys are being used as gas turbine materials because of their superior creep strength at high temperatures. The excellent mechanical property of these alloys originates from the cuboidal γ' strengthening phase that coherently precipitates in the γ phase [1]. In case of the commercial CMSX-4 alloy, the γ/γ' lattice misfit is negative ($a_\gamma > a_{\gamma'}$), and the γ' particles coarsen toward the direction perpendicular to the [001] tensile stress axis during high-temperature creep. This phenomenon is known as “rafting” [2]. Phase-field simulation studies have revealed that the main driving force for rafting is the plasticity in the γ phase [3–8]. This suggests that the microstructure evolution and creep deformation are strongly correlated, and both need to be simultaneously modeled in the microstructure-dependent creep analysis.

Recently, a phase-field model has been developed that considers both the morphological change in the γ' phase and the microstructure-dependent heterogeneous creep in the γ phase [9]. Two- (2D) and three-dimensional (3D) simulations based on this model can reproduce the rafting phenomenon [9,10]. However, because of the difficulty in estimating the diffusion mobility associated with γ/γ' interface migration (hereafter referred to as the γ/γ' diffusion mobility), it is necessary to fit the simulated and experimental creep response data to correlate the reduced time in the simulation with the actual time [9,10]. In this study, we have estimated the γ/γ' diffusion mobility in CMSX-4 from the database of multicomponent atomic diffusion mobility. This estimation is based on the assumption that the γ/γ' interface migration is controlled by the atomic diffusion of the element that exhibits the smallest atomic diffusion mobility in an alloy system under consideration. On the basis of a phase-field simulation study, we have confirmed that the estimated γ/γ' diffusion mobility can be effectively utilized for the 3D phase-field simulation of rafting in CMSX-4.

2. Calculation method

2.1 Phase-field model

In this study, we have adopted the phase-field model developed by Tsukada et al. [9]. To describe the ($\gamma + \gamma'$) microstructure, the local volume fraction of the γ' phase $f(\mathbf{r}, t)$ and the structural-order parameter fields, which distinguish four different ordered domains in the γ' phase $\phi_i(\mathbf{r}, t)$ with $i = 1, 2, 3, 4$, are employed. These field variables are functions of space (\mathbf{r}) and time (t). It is assumed that the local volume fraction $f(\mathbf{r}, t)$ is related to the concentration field $c(\mathbf{r}, t)$ as follows:

$$f(\mathbf{r}, t) = \frac{c(\mathbf{r}, t) - {}^0c^{(\gamma)}}{{}^0c^{(\gamma')} - {}^0c^{(\gamma)}}. \quad (1)$$

Here ${}^0c^{(\gamma)}$ and ${}^0c^{(\gamma')}$ are the equilibrium concentrations in the γ and γ' phases, respectively. The temporal evolution of the field variables is given by the Cahn–Hilliard and Allen–Cahn equations as follows [11]:

$$\frac{\partial f(\mathbf{r}, t)}{\partial t} = M_f \nabla^2 \frac{\delta G}{\delta f(\mathbf{r}, t)}, \quad (2)$$

$$\frac{\partial \phi_i(\mathbf{r}, t)}{\partial t} = -L \frac{\delta G}{\delta \phi_i(\mathbf{r}, t)}, \quad i = 1, 2, 3, 4, \quad (3)$$

where G is the total free energy of the microstructure, M_f is the γ/γ' diffusion mobility, and L is the structural relaxation coefficient. The total free energy is described as [9,12]

$$G = \int_r \left[\{1 - h(\phi_i)\} G^{(\gamma)}(f^{(\gamma)}) + h(\phi_i) G^{(\gamma')} (f^{(\gamma')}) + wg(\phi_i) + \frac{\kappa_\phi}{2} (\nabla \phi_i)^2 \right] d\mathbf{r} + E_{\text{el}},$$

$$h(\phi_i) = \sum_{i=1}^4 \left[\phi_i^3 (10 - 15\phi_i + 6\phi_i^2) \right],$$

$$g(\phi_i) = \sum_{i=1}^4 \left[\phi_i^2 (1 - \phi_i)^2 \right] + \alpha \sum_{i=1}^4 \sum_{j \neq i}^4 \phi_i^2 \phi_j^2.$$

Here $G^{(\gamma)}$ and $G^{(\gamma')}$ are the Gibbs energy densities of the γ and γ' phases, respectively, and are approximated as $G^{(\gamma)} = W^{(\gamma)} f^2$ and $G^{(\gamma')} = W^{(\gamma')} (1 - f)^2$, respectively; $W^{(\gamma)}$ and $W^{(\gamma')}$ are the energy coefficients estimated from the thermodynamic database of the phase diagrams. As suggested in the model proposed by Kim et al. [13], the γ/γ' interface region is regarded as a mixture of the γ and γ' phases with different γ' volume fractions, $f^{(\gamma)}$ and $f^{(\gamma')}$, but with equal chemical potentials [9,13]. The parameter w is the double-well potential height, κ_ϕ is the gradient energy coefficient [14], and E_{el} is the elastic strain energy. The parameters w and κ_ϕ are related to both the γ/γ' interfacial energy (γ_s) and the interface thickness (2λ) as $\gamma_s = \sqrt{w\kappa_\phi} / 3\sqrt{2}$ and $2\lambda = \alpha \sqrt{2\kappa_\phi} / w$. Similarly, the coefficient α depends on the definition of 2λ and is set to $\alpha = 2$ [14]. Meanwhile, the elastic strain energy E_{el} is given by [15,16]

$$E_{\text{el}} = \int_r \left[\frac{1}{2} C_{ijkl}(\mathbf{r}, t) \{ \varepsilon_{ij}(\mathbf{r}, t) - \varepsilon_{ij}^0(\mathbf{r}, t) \} \{ \varepsilon_{kl}(\mathbf{r}, t) - \varepsilon_{kl}^0(\mathbf{r}, t) \} - \sigma_{ij}^{\text{appl}} \bar{\varepsilon}_{ij} \right] d\mathbf{r},$$

where C_{ijkl} is the elastic constant, ε_{ij} is the total strain, ε_{ij}^0 is the eigenstrain, $\sigma_{ij}^{\text{appl}}$ is the applied stress, and $\bar{\varepsilon}_{ij}$ is the uniform macroscopic strain. On the basis of the mechanical equilibrium equation, the total strain ε_{ij} is calculated from the spatial distribution of the

eigenstrain under the stress-controlled boundary condition. The eigenstrain is defined by [9]

$$\varepsilon_{ij}^0(\mathbf{r}, t) = \varepsilon_0 \delta_{ij} h(\phi_i) + \varepsilon_{ij}^p(\mathbf{r}, t) + \varepsilon_{ij}^c(\mathbf{r}, t),$$

where δ_{ij} is the Kronecker delta function and ε_0 is the lattice misfit calculated from the lattice parameter of each phase defined as $\varepsilon_0 \equiv (a^{(\gamma')} - a^{(\gamma)}) / a^{(\gamma)}$. The terms ε_{ij}^p and ε_{ij}^c are the plastic and creep strains, respectively, and both are confined to the γ' phase. That is, the γ' phase is regarded as an elastic body in the simulation. The evolution of ε_{ij}^p is calculated by iteratively solving the following equation [17] until the equivalent stress in the entire γ' -phase region becomes less than the yield stress:

$$\frac{\partial \varepsilon_{ij}^p(\mathbf{r}_p, t)}{\partial t} = -K_{ijkl} \frac{\delta E_{\text{shear}}}{\delta \varepsilon_{kl}^p(\mathbf{r}_p, t)}. \quad (4)$$

Here K_{ijkl} is the kinetic coefficient and E_{shear} is the shear strain energy. For simplicity, K_{ijkl} is assumed to be $K_{ijkl} = K \delta_{ik} \delta_{jl}$. Eq. (4) is solved only at \mathbf{r}_p where the von Mises yield criterion is exceeded. E_{shear} is given by

$$E_{\text{shear}} = \int_r \left[\frac{1}{2} C_{ijkl}(\mathbf{r}, t) \{e_{ij}(\mathbf{r}, t) - e_{ij}^0(\mathbf{r}, t)\} \{e_{kl}(\mathbf{r}, t) - e_{kl}^0(\mathbf{r}, t)\} - s_{ij}^{\text{appl}} \bar{e}_{ij} \right] d\mathbf{r},$$

where e_{ij} and s_{ij} correspond to the deviatoric strain and deviatoric stress, respectively. The evolution of ε_{ij}^c is calculated on the basis of the creep theory of the von Mises type [9,18]:

$$\frac{\partial \varepsilon_{ij}^c(\mathbf{r}, t)}{\partial t} = \frac{3}{2} C \bar{\sigma}^4(\mathbf{r}, t) s_{ij}(\mathbf{r}, t), \quad (5)$$

where C is the creep coefficient and $\bar{\sigma}$ is the equivalent stress.

2.2 γ/γ' diffusion mobility

The γ/γ' diffusion mobility in Eq. (2) is estimated as follows. In case of multicomponent systems, concentration fields ($c_i(\mathbf{r}, t)$) are often employed as field variables, and their temporal evolution is calculated by solving the following equation [19]:

$$\frac{\partial c_i(\mathbf{r}, t)}{\partial t} = \nabla \left(M_{im} \nabla \left(\frac{\delta G}{\delta c_m(\mathbf{r}, t)} \right) \right), \quad (6)$$

where M_{im} is the atomic diffusion mobility of species i with respect to the diffusion potential gradient of element m . Assuming that the atomic diffusion mobility is constant at a constant temperature and ignoring the cross terms of the diffusion potential gradient, Eq. (6) is rewritten as

$$\frac{\partial c_i(\mathbf{r}, t)}{\partial t} = M_{ii} \nabla^2 \left(\frac{\delta G}{\delta c_i(\mathbf{r}, t)} \right). \quad (7)$$

Hence, the following equation is derived from Eqs. (1) and (7) for all the diffusion species:

$$\frac{\partial f(\mathbf{r}, t)}{\partial t} = \frac{M_{ii}}{({}^0c_i^{(\gamma')} - {}^0c_i^{(\gamma)})^2} \nabla^2 \frac{\delta G}{\delta f(\mathbf{r}, t)}, \quad (8)$$

where ${}^0c_i^{(\gamma)}$ and ${}^0c_i^{(\gamma')}$ are the equilibrium concentrations of species i in the γ and γ' phases,

1 respectively. Note that, the Einstein summation convention is not applied in Eq. (8). The
 2 values of M_{ii} at 1273 K are listed in Table 1, which are calculated for the alloy composition
 3 of CMSX-4 [20]. The calculations are based on the database of multicomponent atomic
 4 diffusion mobility for nickel-based superalloys [21]. It is seen that the atomic diffusion
 5 mobility of Re M_{ReRe} has the smallest value. Because it is assumed that the phase
 6 equilibrium can be almost reached during high-temperature creep, it is presumed that the γ/γ'
 7 interface migration is controlled by the atomic diffusion of Re. Consequently, from the
 8 chemical compositions of the γ and γ' phases [20], the γ/γ' diffusion mobility is estimated as

$$M_f = \frac{M_{\text{ReRe}}}{(c_{\text{Re}}^{(\gamma')} - c_{\text{Re}}^{(\gamma)})^2}. \quad (9)$$

2.3 Simulation conditions

27
 28
 29
 30
 31
 32 3D simulations were performed by numerically solving Eqs. (2), (3), (4), and (5) by
 33 the difference method. The number of computational cell is $32 \times 32 \times 32$, and the system size
 34 is $256 \times 256 \times 256 \text{ nm}^3$. Figure 1 shows the initial microstructure of the simulation; the
 35 cuboidal γ' phase with an edge length of approximately 200 nm is placed at the center of the
 36 computational cell. The periodic boundary conditions are assumed along all the three
 37 dimensions. The parameters used in the simulation are summarized in Table 2. The values of
 38 $W^{(\gamma)}$ and $W^{(\gamma')}$ are estimated using the thermodynamic database of the Ni–Al system [22].
 39 This approximation is reasonable because our simulation focuses on the rafting phenomenon
 40 in the later stages of γ' coarsening. The parameters w and κ_ϕ are fitted to a γ/γ' interfacial
 41 energy of $\gamma_s = 0.0142 \text{ J m}^{-2}$ [23]. The elastic constants and lattice parameters of CMSX-4 at
 42 1273 K are considered as reported in the literature [20,24]. The local elastic constant is
 43 assumed to be $C_{ijkl}(\mathbf{r}) = \{1 - h(\phi_i)\} C_{ijkl}^{(\gamma)} + h(\phi_i) C_{ijkl}^{(\gamma')}$, and an iterative perturbation approach is

1 adopted for solving the inhomogeneous elasticity equation [25]. Because of the lack of
2 experimental data, the structural relaxation coefficient L in Eq. (3) is not well determined
3 and is set to be sufficiently large to ensure that the microstructure evolution is diffusion
4 controlled.
5
6
7
8
9

10 11 **3. Results and discussion**

12
13
14
15
16 Figure 2 shows the 3D simulation results of CMSX-4 at 1273 K under a tensile stress
17 of 160 MPa along the [001] direction. Figure 2 (a) shows the microstructure, while Figs. 2 (b)
18 and (c) indicate the 3D contours of the equivalent inelastic strain rate ($\dot{\bar{\epsilon}}_p + \dot{\bar{\epsilon}}_c$) and the
19 equivalent inelastic strain ($\bar{\epsilon}_p + \bar{\epsilon}_c$), respectively. As evidenced from the figure, the γ' phase
20 evolves toward the direction perpendicular to the [001] tensile stress axis. Inelastic strain is
21 preferentially large in the horizontal γ channels (Fig. 2 (c)). This result is consistent with that
22 reported on the dislocation preference in the γ channels [3]. Because the periodic array of the
23 γ' particles is assumed to be along the $\langle 100 \rangle$ directions in the simulation, the γ' phase
24 connects with the neighboring particles through directional coarsening, and the vertical γ
25 channels disappear at $t = 9\text{--}10$ h. At this moment, the microstructure-dependent
26 heterogeneous creep is clearly observed, and the inelastic strain rate temporarily increases in
27 the wide range of the γ -phase region (Fig. 2 (b)). In the experiment, it is assumed that the
28 rafting starts before $t = 30$ h [9], which is well reproduced by our simulation. After the (001)
29 rafted structure is formed at approximately $t = 15$ h, the microstructure evolution does not
30 occur in the simulation.
31
32
33
34
35
36
37
38
39
40
41
42
43
44
45
46
47
48
49

50
51 Figure 3 shows the macroscopic creep rate–time curve for CMSX-4 at 1273 K under
52 a tensile stress of 160 MPa along the [001] direction. In the figure, the solid and open symbols
53 represent the simulation results and experimental data [26], respectively. The decrease in
54 creep rate during the initial stage of creep is quantitatively reproduced in the simulation. The
55
56
57
58
59
60
61
62
63
64
65

1 macroscopic creep behavior is influenced by the microstructure evolution, and a temporary
2 increase in the creep rate originating from rafting is observed in the simulation, as indicated
3 by the arrow in Fig. 3. After the temporary increase, the creep rate continues to decrease in the
4 simulation, whereas an accelerating creep stage is observed in the experiment. This
5 discrepancy between the simulated and experimental curves can be attributed to the fact that
6 the simulation does not reproduce the coalescence of the (001) rafted structure [27]. The
7 experimentally observed acceleration of creep can be attributed to the increase in the
8 γ -channel width of the rafted structure [26]. Therefore, for predicting creep rupture life on the
9 basis of microstructure evolution, another phase-field model that can simulate the widening of
10 the rafted structure in the accelerating creep stage is needed.

23 In this study, instead of solving Cahn–Hilliard equations of all diffusion species,
24 temporal evolution of the γ' volume fraction field is solved for simplicity (Eq. (2)) because we
25 assume that the phase equilibrium is reached during high-temperature creep; hence, the
26 partitioning behavior of solutes between the γ and γ' phases during creep does not need to be
27 solved. The rafting phenomenon is a diffusion-controlled process; hence, the estimation of γ/γ'
28 diffusion mobility in Eq. (2) is essential for the quantitative phase-field simulation of rafting,
29 while the accurate value of L in Eq. (3) is not required as long as it is sufficiently large. As
30 given by Eq. (9), the γ/γ' diffusion mobility can be estimated from the database of atomic
31 diffusion mobility by assuming that the γ/γ' interface migration is controlled by the atomic
32 diffusion of Re, which exhibits the smallest atomic diffusion mobility in CMSX-4. Our
33 simulation based on the estimated value of M_f could reproduce the experimental data on
34 macroscopic creep rate–time curve of CMSX-4 in the initial stage of creep, as shown in Fig. 3
35 and succeeded in the quantitative analysis of rafting kinetics. Hence, our assumption that the
36 phase equilibrium is reached during creep and microstructure evolution is controlled by the
37 atomic diffusion of Re is reasonable. The addition of Re reduces the γ/γ' diffusion mobility
38 and hence can suppress the evolution of $(\gamma + \gamma')$ microstructure during high-temperature creep.

1 This leads to a dramatic improvement in the creep rupture life of superalloys [1]. Except for
2 Re, the values of atomic diffusion mobility of W, Ta, and Mo are comparatively smaller in
3 CMSX-4, as shown in Table 1. Hence, it is assumed that these elements also contribute to the
4 suppression of microstructure evolution during creep. This is not surprising because it is a
5 well-known fact that not only Re but also W, Ta, and Mo are creep-strengthening elements in
6 single-crystal superalloys [1]. For controlling the γ/γ' diffusion mobility given by Eq. (9), the
7 optimization of alloy chemistry to reduce M_{ReRe} and the prediction of equilibrium
8 concentrations of Re in the γ and γ' phases at a creep temperature are assumed to be
9 important.
10
11
12
13
14
15
16
17
18
19
20
21
22

23 4. Conclusions

24
25
26
27 The γ/γ' diffusion mobility was estimated from the database of multicomponent
28 atomic diffusion mobility by assuming that the phase equilibrium is reached during
29 high-temperature creep, and the γ/γ' interface migration is controlled by the atomic diffusion
30 of Re. Using a phase-field simulation based on the estimated γ/γ' diffusion mobility, we
31 analyzed the microstructure-dependent creep of CMSX-4 at 1273 K under a tensile stress of
32 160 MPa. The rafting phenomenon, microstructure-dependent heterogeneous creep, and
33 macroscopic creep response were well reproduced by the simulation. The simulated
34 macroscopic creep rate–time curve in the initial stage of creep was consistent with
35 experimental data, and we succeeded in the quantitative analysis of the rafting kinetics. The
36 estimation of the γ/γ' diffusion mobility is assumed to be effective for quantitatively analyzing
37 the microstructure evolution during high-temperature creep by the phase-field simulation.
38
39
40
41
42
43
44
45
46
47
48
49
50
51
52
53
54
55
56
57
58
59
60
61
62
63
64
65

References

- [1] R. C. Reed, *The Superalloys Fundamentals and Applications*, Cambridge University Press, New York, 2006.
- [2] T. M. Pollock, A.S. Argon, *Acta Metall. Mater.* 42 (1994) 1859–1874.
- [3] N. Zhou, C. Shen, M. J. Mills, Y. Wang, *Acta Mater.* 55 (2007) 5369–5381.
- [4] Y. Tsukada, Y. Murata, T. Koyama, M. Morinaga, *Mater. Tras.* 49 (2008) 484–488.
- [5] N. Zhou, C. Shen, M. J. Mills, Y. Wang, *Acta Mater.* 56 (2008) 6156–6173.
- [6] N. Zhou, C. Shen, P. M. Sarosi, M. J. Mills, T. Pollock, Y. Wang, *Mater. Sci. Technol.* 25 (2009) 205–212.
- [7] A. Gaubert, Y. Le Bouar, A. Finel, *Philos. Mag.* 90 (2010) 375–404.
- [8] Y. Tsukada, Y. Murata, T. Koyama, M. Morinaga, in: J. Lecomte-Beckers, Q. Contrepois, T. Beck, B. Kuhn (Eds.), *Materials for Advanced Power Engineering 2010* (Proceeding of the 9th Liège conference), Forschungszentrum Jülich, Jülich, 2010, pp. 759–768.
- [9] Y. Tsukada, Y. Murata, T. Koyama, N. Miura, Y. Kondo, *Acta Mater.* 59 (2011) 6378–6386.
- [10] Y. Tsukada, Y. Murata, T. Koyama, N. Miura, Y. Kondo, in: E. S. Huron, R. C. Reed, M. C. Hardy, M. J. Mills, R. E. Montero, P. D. Portella, J. Telesman (Eds.), *Superalloys 2012* (Proceedings of the 12th international symposium on superalloys), John Wiley & Sons, Inc., Hoboken, 2012, pp. 111–119.
- [11] L. Q. Chen, *Annu. Rev. Mater. Res.* 32 (2002) 113–140.
- [12] J. Z. Zhu, T. Wang, A. J. Ardell, S. H. Zhou, Z. K. Liu, L. Q. Chen, *Acta Mater.* 52 (2004) 2837–2845.
- [13] S. G. Kim, W. T. Kim, T. Suzuki, *Phys. Rev. E* 60 (1999) 7186–7197.

- 1 [14] J. W. Cahn, J. E. Hilliard, *J. Chem. Phys.* 28 (1958) 258–267.
2
3 [15] T. Mura, *Micromechanics of Defects in Solids*, 2nd rev. ed., Kluwer Academic,
4 Dordrecht, 1987.
5
6 [16] A. G. Khachaturyan, *Theory of Structural Transformations in Solids*, Dover, New York,
7 2008.
8
9 [17] X. H. Guo, S. Q. Shi, X. Q. Ma, *Appl. Phys. Lett.* 87 (2005) 221910.
10
11 [18] F. K. G. Odqvist, *Mathematical Theory of Creep and Creep Rupture*, Oxford University
12 Press, London, 1966.
13
14 [19] T. Kitashima, H. Harada, *Acta Mater.* 57 (2009) 2020–2028.
15
16 [20] D. Siebörger, H. Knake, U. Glatzel, *Mater. Sci. Eng. A* 298 (2001) 26–33.
17
18 [21] C. E. Campbell, W. J. Boettinger, U. R. Kattner, *Acta Mater.* 50 (2002) 775–792.
19
20 [22] I. Ansara, N. Dupin, H. L. Lukas, B. Sundman, *J. Alloys Compd.* 247 (1997) 20–30.
21
22 [23] A. J. Ardell, *Acta Metall.* 16 (1968) 511–516.
23
24 [24] U. Glatzel, *Scripta Metall. Mater.* 31 (1994) 291–296.
25
26 [25] S. Y. Hu, L. Q. Chen, *Acta Mater.* 49 (2001) 1879–1890.
27
28 [26] N. Miura, Y. Kondo, T. Matsuo, *Tetsu To Hagane* 89 (2003) 1240–1247.
29
30 [27] K. Serin, G. Göbenli, G. Eggeler, *Mater. Sci. Eng. A* 387–389 (2004) 133–137.
31
32
33
34
35
36
37
38
39
40
41
42
43
44
45
46
47
48
49
50
51
52
53
54
55
56
57
58
59
60
61
62
63
64
65

1
2
3 Captions:
4
5
6

7 Table 1 Atomic diffusion mobility M_{ii} at 1273 K calculated for the alloy composition of
8
9 CMSX-4.
10

11
12
13
14 Table 2 Parameters used in the 3D phase-field simulation.
15
16

17
18 Fig. 1 Initial microstructure of the 3D phase-field simulation. The cube at the center of the
19
20 computational cell is the γ' phase.
21
22

23
24
25 Fig. 2 3D phase-field simulation results of CMSX-4 at 1273 K under a tensile stress of 160
26
27 MPa along the [001] direction: (a) microstructure, (b) 3D contours of the inelastic strain rate
28
29 ($\dot{\bar{\epsilon}}_p + \dot{\bar{\epsilon}}_c$), and (c) 3D contours of the inelastic strain ($\bar{\epsilon}_p + \bar{\epsilon}_c$).
30
31
32

33
34
35 Fig. 3 Creep rate–time curve for CMSX-4 at 1273 K under a tensile stress of 160 MPa along
36
37 the [001] direction. The solid and open symbols represent the simulation results and
38
39 experimental data, respectively.
40
41
42
43
44
45
46
47
48
49
50
51
52
53
54
55
56
57
58
59
60
61
62
63
64
65

Table 1

[Click here to download high resolution image](#)

Diffusion species, <i>i</i>	Ni	Al	Co	Cr	Mo	Ta	Re	W	Hf	Ti
Mobility, $M_{ii} / J^{-1} \text{ mol m}^2 \text{ s}^{-1}$	2.43×10^{-20}	2.68×10^{-20}	5.14×10^{-21}	7.77×10^{-21}	2.58×10^{-22}	9.75×10^{-22}	1.94×10^{-23}	1.50×10^{-22}	8.23×10^{-22}	1.33×10^{-21}

Table 2

[Click here to download high resolution image](#)

γ/γ' diffusion mobility, M_f ($\text{J}^{-1} \text{mol m}^2 \text{s}^{-1}$)	2.15×10^{-20}
Gibbs energy coefficients, W (J m^{-3})	$W^{(\gamma)} = 1.29 \times 10^8$, $W^{(\gamma')} = 1.56 \times 10^8$
Double-well potential height, w (J m^{-3})	1.07×10^7
Gradient energy coefficient, κ_ϕ (J m^{-1})	3.41×10^{-10}
Elastic constants, C_{ijkl} (GPa)	$C^{(\gamma)}_{11} = 204.9$, $C^{(\gamma)}_{12} = 150.8$, $C^{(\gamma)}_{44} = 94.0$ $C^{(\gamma')}_{11} = 251.6$, $C^{(\gamma')}_{12} = 194.5$, $C^{(\gamma')}_{44} = 95.0$
Lattice misfit, ε_0	-0.0023
Yield stress of the γ phase, σ_y (MPa)	120
Creep coefficient, C ($\text{MPa}^{-5} \text{s}^{-1}$)	6.64×10^{-18}

Figure 1
[Click here to download high resolution image](#)

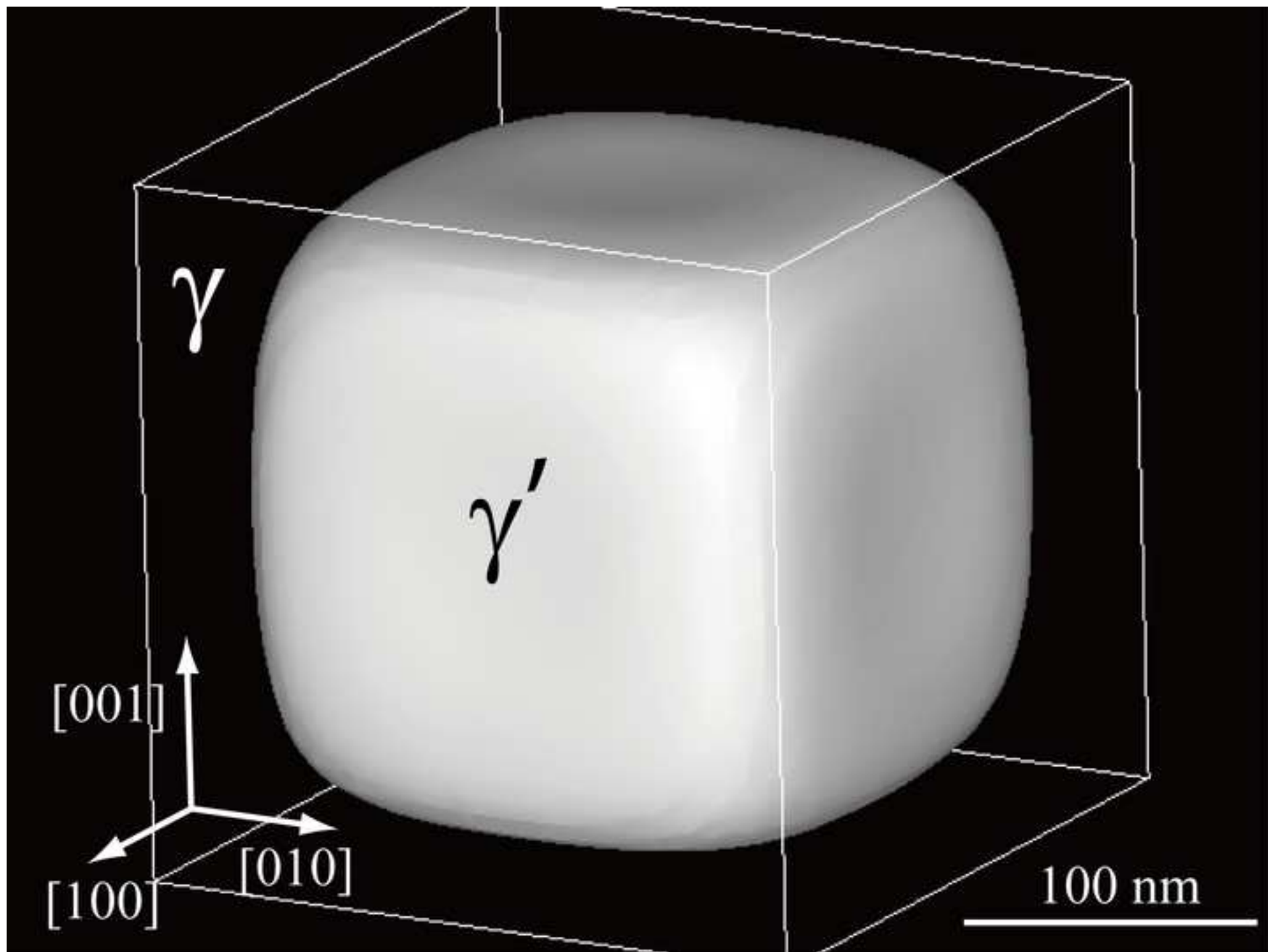


Figure 2
[Click here to download high resolution image](#)

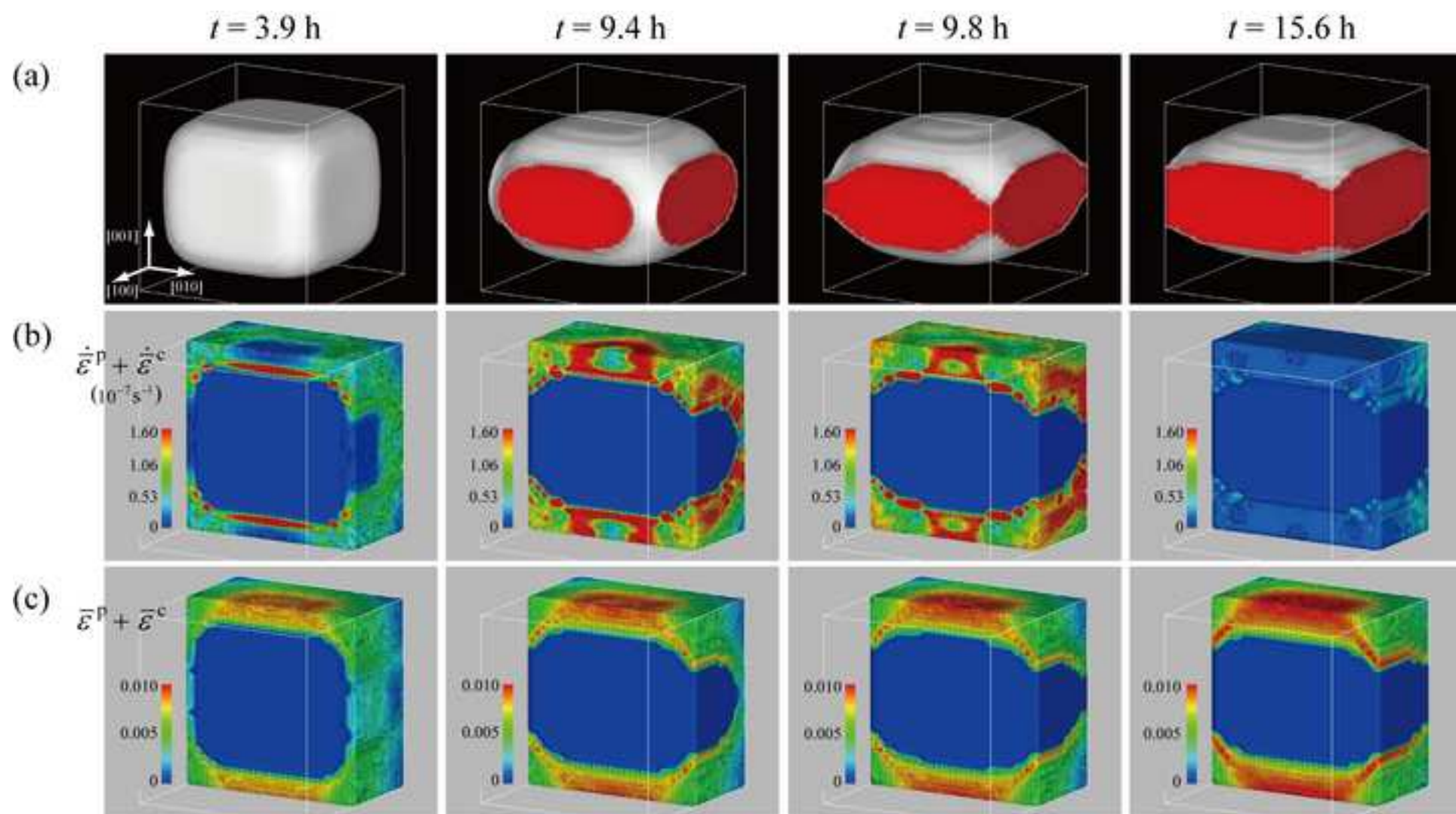


Figure 3
[Click here to download high resolution image](#)

